ACS APPLIED MATERIALS & INTERFACES

Research Article

www.acsami.org

Controllable Occurrence of Free-Standing Lipid Membranes on Nanograting Structured Supports

Po-Yu Peng, Po-Chieh Chiang, and Ling Chao*

Department of Chemical Engineering, National Taiwan University, Taipei 106, Taiwan

Supporting Information

ABSTRACT: Supported lipid bilayers (SLBs) have been widely used to study protein−lipid membrane interactions because their planar geometry is suitable for many surface analysis tools. However, the friction coupling between the support and the membrane can influence the properties of biomolecules in the membrane. Many studies have attempted to span SLBs over nanostructured supports to create free-standing regions in SLBs for biosensor applications. However, membranes following the support surface contour are more frequently observed than are free-standing membranes on structured supports, indicating that the parameter range suitable for formation of free-standing SLBs might be narrow and more information is necessary to understand the required conditions. The objective of this study was to estimate the system energies of free-standing and contour-following membrane states and determine which state is the most energetically favorable under various conditions. For a lipid membrane preferring to stay close to the support, an energy reward occurs when they are in close proximity; however, increasing the contact area on a structured surface can result in an energy penalty because of the bending of the lipid bilayer. Whether the energy reward or the energy penalty dominates could determine the membrane state. We used the extended Derjaguin−Landau−Verwey−Overbeek (DLVO) theory and the Helfrich bending theory to relate the energy sizes to experimentally controllable parameters. We experimentally examined whether the membrane state followed the model prediction when we used various buffer ionic strengths, various lipid types, and nanograting supports with three different geometries. Because it is difficult to observe the experimental membrane state directly at the nanoscale, we developed a method to use the fluorescence recovery shape change after photobleaching to distinguish experimental membrane states at the micrometer scale. Our experimental results closely matched the theoretical predictions, suggesting that the developed model can be used to predict suitable conditions for formation of free-standing bilayers on nanostructured solid supports.

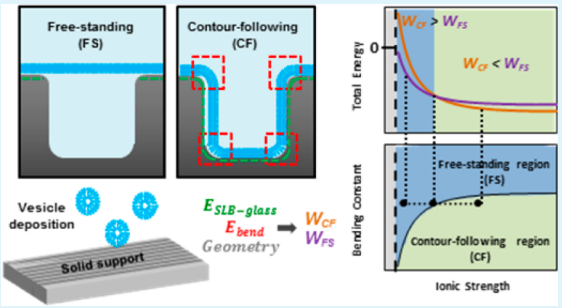

KEYWORDS: *supported lipid bilayers, nanograting structured support, trench-spanning membranes, free-standing, contour-following, extended DLVO theory*

INTRODUCTION

Lipid membranes have been shown to play critical roles in influencing membrane protein structure and function. Supported lipid bilayers (SLBs) have been widely used as a biomimetic platform for studying lipid-membrane-associated cellular processes in vitro. SLBs are planar extended bilayers adsorbed on suitable solid surfaces,[1,2] and the planar geometry position is compatible with a wide range of surface analysis tools requiring planar geometry.[3−5] An SLB can retain their fluid property by trapping a thin water layer between the solid support and the lipid bilayer.[6−8] In addition, many studies have successfully incorporated cell membrane functional components, such as proteins, onto or into SLBs.[9,10] However, a major shortcoming of an SLB is the short 1−2 nm distance from the solid support and that the friction coupling can cause slower diffusion of a biomolecule in the membrane.[11] Although the free-spanning black lipid membrane (BLM)[12,13] has been developed as another type of biomimetic membrane platform, it has poor stability[14] and the solvent remaining in the lipid bilayer during preparation influences the properties of the biomolecules embedded in the membrane.

To overcome the solid support effect and solvent residue problem, many studies have attempted to span SLBs over supports with holes or trenches to create free-standing regions in the lipid bilayers. Studies have ruptured the giant unilamellar vesicles (GUVs) on supports with submicrometer holes, and the lipid bilayer tension can keep them spanning over the holes;[15−19] however, forming a large-area continuous planar SLB by depositing GUVs is difficult, and the partial coverage of lipid bilayers on the support can limit its applications. Other studies have used a large unilamellar vesicle deposition method to create a continuous SLB;[20,21] however, the method requires the vesicle size to be substantially larger than the spanned pore size, and the percentage of successfully spanned pores depends

Received: March 27, 2014
Accepted: July 2, 2014
Published: July 2, 2014

on the frequency of occurrence of a vesicle positioning itself over the pore region during the vesicle deposition method.[21] Furthermore, Jönssön et al. use a shear force from the bulk flow in a microfluidic device to drive the movement of a preformed SLB to span nanowells. However, a high pH value (pH = 9.5) bulk solution is required to allow the SLB to span the wells, and the lipid bilayer follows the contour of the wells at lower pH values.[22] The rare observations of stable free-standing bilayers on submicrometer or nanostructured supports indicate that the parameter range suitable for formation of free-standing lipid bilayers is narrow and more information is required to understand the suitable conditions.

Studies have often revealed that support surface contour following is a more stable state for SLBs under many physiologically relevant conditions.[23−25] For a lipid membrane preferring to stay close to the support, an attraction occurs between the support and the lipid bilayer, and increasing the contact area can increase the energy reward of the system. However, increasing the contact area on a structured surface can result in bending of the lipid bilayer, which can cause an energy penalty to the system.[21,26] Whether the energy reward or the energy penalty dominates determines whether the membrane follows the support surface contour or forms free-standing membrane without bending. However, recent studies have focused on reporting the conditions that can create free-standing membranes, and the membrane state seems to be sensitive to operating conditions. A more comprehensive study is required to determine whether a free-standing membrane can form under the given conditions or how to adjust the experimentally controllable conditions to obtain a free-standing membrane.

In this study, we developed a theoretical model to estimate the membrane states under various conditions and developed an experimental approach to examine whether the experimentally obtained membrane states are consistent with those predicted by the model. The model describes the energies of various membrane states based on the extended Derjaguin−Landau−Verwey−Overbeek (DLVO) theory and the Helfrich bending theory and can estimate how the membrane state can be influenced by the solid support geometry or by biologically relevant parameters, such as ionic strength and the membrane bending constant. We conducted experiments under various conditions and experimentally examined the membrane states by the fluorescence recovery after photobleaching technique. The consistency between the experimental results and the parameter region predicted by the theory suggested that the model can be used to further estimate the suitable conditions for creating free-standing membranes. Because the membrane state depends on the delicate interaction balance between the support and the lipid membrane and is sensitive to biological conditions, this model can act as a guideline for predicting the membrane state under various conditions or constraints.

MATERIALS AND METHODS

Materials. 1,2-Dioleoyl-*sn*-glycero-3-phosphocholine (DOPC), 1,2-dimyristoyl-*sn*-glycero-3-phosphocholine (DMPC), 1,2-dipalmitoyl-*sn*-glycero-3-phosphocholine (DPPC), 1-stearoyl-2-oleoyl-*sn*-glycero-3-phosphocholine (SOPC), and cholesterol (Chol) were purchased from Avanti Polar Lipids (Alabaster, AL, USA) and used without further purification. 1,2-Dihexadecanoyl-*sn*-glycero-3-phosphoethanol amine triethylammonium salt (Texas Red DHPE) was purchased from Life Technologies (Grand Island, NY, USA). All other reagents, unless otherwise specified, were purchased from Sigma-Aldrich (St. Louis, MO, USA). Fused silica slides were purchased from Precision Glass & Optics (Santa Ana, CA, USA).

Preparation of Nanograting Structure Fused Silica. The fused silica solid supports with a nanograting structure were fabricated through nanoimprinting lithography. The silicon molds with 208 nm line grating width (LightSmyth Technology, OR, USA) were used to create a nanograting structure on a 200 nm poly(methyl methacrylate) (PMMA) resist layer covering fused silica solid supports (Corning, NY, USA). Nanoimprinting was performed using a Nanoimprinter (NIL-3.0 Imprinter, Obducat AB, Sweden) at 180 °C, 50 bar for 5 min. After transferring the mold geometry to the resist layer, the reactive ion etching (RIE) technique was applied to remove the thin part of the resist layer while the thick part remained on the support. Subsequently, a 10 nm chromium (Cr) layer was deposited onto the entire substrate. Part of the Cr layer was deposited on the exposed fused silica substrate where the above resist layer had been removed, and the other part of the Cr layer was deposited on the residual photoresist layer. The entire substrate was placed in the solvent to remove the residual photoresist layer from the substrate. After removal, only the Cr layer directly deposited on the solid support remained on the fused silica substrate. The exposed fused silica region which was not masked by the Cr layer was further etched to the desired height using the RIE instrument (Oxford Instruments, Plasmalab 80 Plus RIE, 200 W, chamber pressure at 50 mTorr, and a mixture of CHF_3 and O_2 at a flow rate of 50/2 sccm). The Cr layer was then removed using a Cr etchant (Cr-7T). Finally, the fused silica substrates with nanograting structures were cleaned in a solution (NH_4OH:H_2O_2:H_2O = 1:1:5) at 80 °C for 10 min.

Substrate Cleaning and Formation of Supported Lipid Membranes. The fused silica substrates were cleaned by immersing them in ethanol under sonication for 1 h, followed by immersion in deionized water under sonication for 1 h. After the sample was removed from the immersion bath and dried using nitrogen, the substrate was placed on a hot plate at 120 °C for 20 min to remove the ethanol or water residue trapped in the grooves of the substrates. Before the lipid vesicle deposition step, the substrate was cleaned using argon plasma for 10 min. Large unilamellar vesicles (LUVs) were prepared for lipid vesicle deposition to form SLBs. In brief, desired lipid mixtures in chloroform were dried using nitrogen and stored in a vacuum for 5 h to remove chloroform. Dried lipid cakes were reconstituted in aqueous solutions at a concentration of 0.2 mg/mL. The reconstitution solutions were pure water with various concentrations of sodium chloride (NaCl) to adjust the solution ionic strength. LUVs were then formed by passing lipid solutions through a 50 nm polycarbonate filter in an Avanti Mini-Extruder (Alabaster, AL, USA). Vesicle solutions were allowed to incubate with the cleaned substrates for 30 min, and the excess vesicles were removed by washing with the same solution used to reconstitute the vesicles.

Fluorescence Photobleaching after Recovery. An intense laser light, 200 mW DPSS Green Laser Module (Unice, Taiwan) at 532 nm, was used to bleach a small spot in a membrane with fluorescently labeled lipid, Texas-Red DHPE, for 0.5 s. The intensity of a bleached spot has a Gaussian profile with an approximate half-maximum width of 10 μm. Recovery images were captured using an inverted microscope (Olympus IX81, Olympus, Japan) equipped with a CCD camera (ORCA-R2, Hamamatsu, Japan). The intensity recovery time in the region of interest was processed using MATLAB (Mathworks Natick, MA, USA) to calculate the two-dimensional diffusion coefficients of the SLB. In brief, the algorithm assumes that the fluorescence intensity is proportional to the concentration of fluorescent molecules, and the diffusion coefficients can be obtained by fitting the data to the two-dimensional classical diffusion equation (eq 1). The initial concentration is assumed to have a Gaussian profile, as described in eq 2; therefore, σ_{x0}, σ_{y0}, c_∞, and α can be obtained by fitting the initial intensity profile to eq 2. Equation 3 was assumed to be able to accurately describe the subsequent concentration profile change. Fitting the subsequent intensity profiles to eq 3 results in the fitted parameters $\sigma_x(t)$ and $\sigma_y(t)$. The diffusion coefficients in the two orthogonal directions on the 2D plane can be further derived using the

equations $\sigma_x^2(t) = \sigma_{x0}^2 + 2D_x t$ and $\sigma_y^2(t) = \sigma_{y0}^2 + 2D_y t$. More details can be found in the Supporting Information.

$$D_x\frac{\partial^2 c}{\partial x^2} + D_y\frac{\partial^2 c}{\partial y^2} = \frac{\partial c}{\partial t} \quad (1)$$

$$c(x, y, t = 0) = c_\infty\left(1 - \alpha\exp\left(-\frac{x^2}{2\sigma_{x0}^2}\right)\exp\left(-\frac{y^2}{2\sigma_{y0}^2}\right)\right) \quad (2)$$

$$c(x, y, t) = c_\infty\left(1 - \alpha\frac{\sigma_{x0}\sigma_{y0}}{\sigma_x(t)\sigma_y(t)}\exp\left(-\frac{x^2}{2\sigma_x(t)^2}\right)\exp\left(-\frac{y^2}{2\sigma_y(t)^2}\right)\right) \quad (3)$$

SEM Measurement of Nanograting Structured Fused Silica. The morphology of the nanograting structured fuse silica was observed using a NOVA NanoSEM 230 from FEI Co. at an operating voltage of 5.0 kV. Images were obtained in a high-vacuum mode. Prior to imaging, the substrate was coated with approximately 2 nm of platinum to render the sample electrically conductive.

RESULT AND DISCUSSION

Total Energies of Various Membrane States on a Trenched Solid Support. A delicate balance of interactions exists between the solid support and the supported lipid bilayer. The type of lipid, solid support properties, and the buffer conditions can substantially influence the state of the supported lipid bilayer. The objective of this study was to estimate the system energies of the previously observed membrane states and determine which state is the most energetically favorable under various conditions. Because previous studies have observed both the contour-following state and the free-standing state in SLBs on nanoto-micrometer-scale structured surfaces, we considered the energies of these two states on nanograting solid supports (Figure 1). Figure 1 illustrates the side view of the two membrane states in one repeating unit of a nanograting array in a solid support perpendicular to the direction along the trenches.

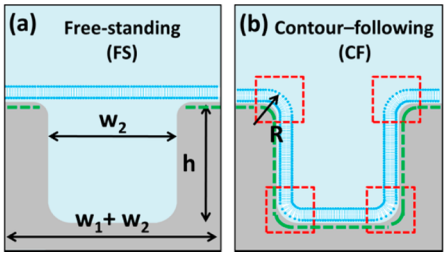

Figure 1. Illustration of the two possible lipid membrane states on a nanograting solid support. Each illustration is the side view of a repeating unit of the trench array. (a) Membrane is in a free-standing (FS) state. (b) Membrane follows the contour of the trench and thus in a contour-following (CF) state. Green lines indicate the contact area between the solid support and the lipid membrane. The larger contact area can render the system more energetically favorable. Red boxes indicate the bending regions, which might make the system energetically unfavorable.

The system energy can be expressed as the combination of the energy reward from the lipid membrane–solid support interaction and the energy penalty from the bending of the membrane. The energy of a free-standing bilayer in water is set as zero. Equations 4 and 5 describe the total energy of the contour-following (CF) and free-standing (FS) membrane states shown in Figure 1a and 1b, respectively

$$W_{CF} = \left(\iint_{A_{SLB}} E_{SLB-silica}\,dA + \iint_{A_{bend}} E_{bend}\,dA\right)/L = (w_1 + w_2 + 2h + 2R(\pi - 4))E_{SLB-silica} + 2R\pi E_{bend} \quad (4)$$

$$W_{FS} = \left(\iint_{A_{SLB}} E_{SLB-silica}\,dA + \iint_{A_{free}} E_{free}\,dA\right)/L = w_1 E_{SLB-silica} \quad (5)$$

where E_{bend} is the bending energy per unit area of the bended lipid bilayer, $E_{SLB-silica}$ is the energy between the silica support surface and the lipid bilayer per unit area of the contact surface, w_1 and w_2 are the upper and lower grating widths respectively, h is the grating height, and R is the radius of the curvature of the grating corner.

A comparison of the size of W_{CF} and W_{FS} can determine which state is the most energetically favorable. On the basis of eqs 4 and 5, the sizes of W_{CF} and W_{FS} can vary based on $E_{SLB-silica}$, E_{bend}, and the support geometry. In this study, we related $E_{SLB-silica}$ to solution ionic strength and the properties of the used lipids, in accordance with the extended DLVO theory,[27−30] and E_{bend} to the radius of the curvature of the support and the bending constants of the used lipids, in accordance with the Helfrich elastic bending theory.[31,32] The intention was to correlate the total energy of each state and the experimentally controllable parameters and therefore to obtain a guideline for the possible conditions to create free-standing membranes.

Using the Extended DLVO Theory To Describe $E_{SLB-silica}$. Previous studies have used the extended DLVO theory to describe the attraction between the lipid membrane and the solid support.[27−30] The summation of the energy contributions from the van der Waals interaction, electrostatic interaction, and hydration interaction determines whether the SLB can form and how strong the affinity is.

The van der Waals force occurs when two substances are in a short distance from each other and is derived from the induced dipole−dipole (orientation) interaction. The van der Waals interaction energy between the oxide surface and the lipid membrane (E_{vdw}) can be expressed as

$$E_{vdw} = -\frac{A}{12\pi}\left(\frac{1}{d^2} - \frac{1}{(d + b)^2}\right) \quad (6)$$

where A is the Hamaker constant for a lipid bilayer interacting with the oxide surface across a water layer, d is the thickness of the water layer, and b is the thickness of the lipid bilayer. The Hamaker constants we used were obtained using the expressions derived from Petrache et al.[33] and Oleson et al.[28] According to their expressions, the Hamaker constant is a function of Debye length (λ_D), water layer thickness (d), and other properties of the oxide surface and the lipid membrane. More details can be found in the Supporting Information.

The next major interaction in the extended DLVO theory is the electrostatic interaction. The electrostatic interaction between the planar oxide surface and the planar lipid membrane can be expressed as

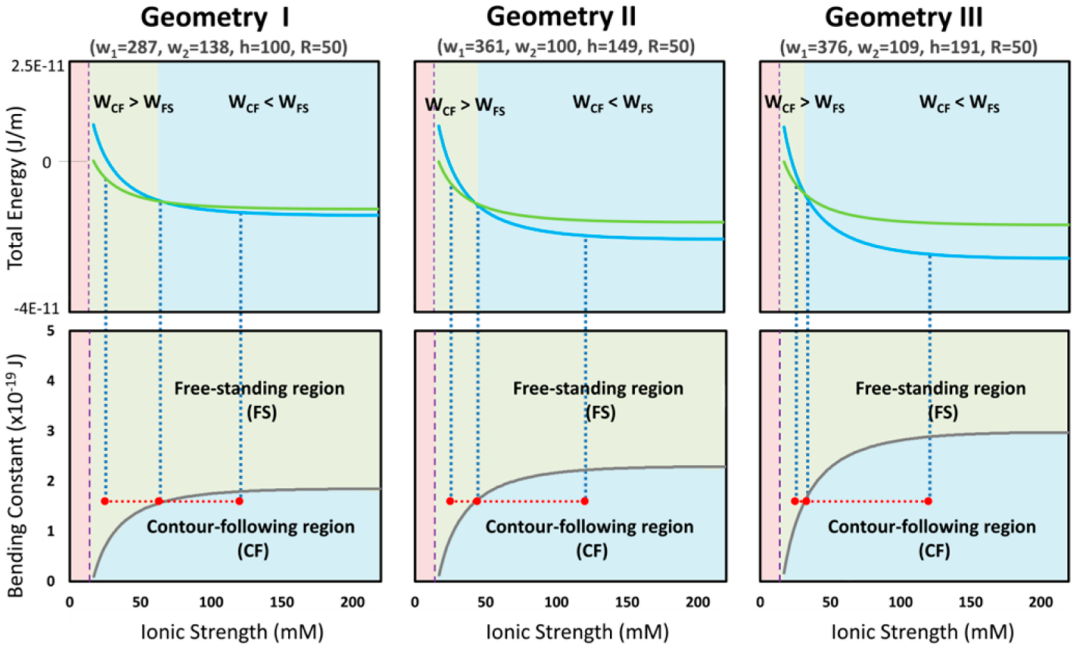

Figure 2. (Top) Typical overall energies of the CF and FS states versus ionic strength calculated with three different support geometries based on the DPPC properties at 43 °C. (Bottom) Theoretical FS and CF state regions on bending constant versus ionic strength diagrams with three different support geometries. The geometry information on Geometries I, II, and III is shown in Figure 3.

$$E_{EDL} = \frac{64c_0k_BT}{\lambda_D}\cdot\tanh\left(\frac{e\psi_S}{4k_BT}\right)\tanh\left(\frac{e\psi_{LB}}{4k_BT}\right)\cdot e^{-d/\lambda_D} \quad (7)$$

where ψ_S and ψ_{LB} are the surface potential of two materials. The variable T is the temperature of the system, k_B is the Boltzmann constant, e is the elementary charge, c_0 is the number density of ions in the bulk solution, d is the support bilayer distance, and λ_D is the Debye length, which is the characteristic thickness of the diffuse electric double layer and can be expressed as

$$\lambda_D = \sqrt{\frac{\varepsilon_0\varepsilon_r k_BT}{2N_Ae^2I}} \quad (8)$$

where k_B is the Boltzmann constant, T is the absolute temperature, N_A is the Avogadro number, e is the elementary charge, ε_0 is the dielectric constant of vacuum, ε_r is the dielectric constant of the electrolyte aqueous solution, and I is the ionic strength of the electrolyte solution.

The third energy contribution is from the hydration interaction.[34] Hydration energy refers to the energy required to remove water from a surface. Formation of a SLB on a hydrophilic surface requires the expulsion of water from the surface; therefore, this third energy contribution is an energy penalty to the system. Because hydration energy is typically measured for two surfaces of the same material, the total hydration energy required to bring an SLB and an oxide support into proximity is assumed to be the average of the hydration energies of the two materials, as shown in eq 9.

$$E_H = \frac{1}{2}\left(l_0p_0\exp\left(\frac{-d}{l_0}\right) + W_0\exp\left(\frac{-d}{\lambda_0}\right)\right) \quad (9)$$

where the first term refers to the hydration energy between two lipid bilayers and the values of l_0 and p_0 can be found in the studies by Israelachvili et al. and McIntosh et al.[35,36] The second term on the right refers to the hydration energy between two oxide solid supports, and W_0 and λ_0 can be found in a previous study.[30]

We assumed that after the supported lipid bilayer forms, the bilayer condition soon reaches equilibrium. The system energy, $E_{overall}$, should be at its lowest value at equilibrium. We defined the system energy at equilibrium as $E_{SLB-silica}$ and the distance between the two materials at equilibrium as d_{min}. The term d_{min} can be obtained by taking the derivative of $E_{overall}$ to distance and setting it to zero because d_{min} is the distance at the minimum energy. Therefore, the energy $E_{SLB-silica}$ can be expressed using eq 10.

$$\begin{aligned} E_{SLB-silica} &= E_{overall}|_{d=d_{min}} \\ &= E_{vdw}|_{d=d_{min}} + E_{EDL}|_{d=d_{min}} + E_H|_{d=d_{min}} \end{aligned} \quad (10)$$

After substituting the parameters that are relatively fixed in this planar bilayer-fused silica system, we determined that $E_{SLB-silica}$ is a function of the buffer ionic strength (I) and the properties of lipid bilayer (such as the surface charge, the bilayer thickness, lipid headgroup area) when the temperature and solid support type are fixed. The detailed expression and parameter settings of $E_{SLB-silica}$ can be found in the Supporting Information.

Using the Helfrich Elastic Bending Theory To Describe E_{bend}. In the Helfrich elastic bending theory, the lipid bilayer is assumed to be a continuous membrane with an elastic bending property. The strength of elastic bending is determined by the bending resistance of materials and the extent of the bending. The bending energy can be expressed as

$$\begin{aligned} E_{bend} &= \int_{membrane}\left\{\frac{1}{2}k(C-c_0)^2 + k_GC_G\right\}dx\,dy \\ &= E_{bend}(k, R) \end{aligned} \quad (11)$$

where C is the curvature, which is the reciprocal of the radius, c_0 is the spontaneous curvature, and C_G is the Gaussian curvature. The terms k and k_G are the bending constant and the Gaussian

bending constant, respectively, and these constants have been reported by Marsh et al. for certain types of lipid membrane.[37] We assumed that the two lipid bilayer leaflets are always symmetric and exert the opposite effect to the curvature; therefore, the spontaneous curvature was set as zero. In addition, only one-dimensional curvature existed in our nanograting solid support; therefore, the Gaussian curvature was set as zero.

Obtaining Theoretical Contour-Following and Free-Standing State Regions for the Prepared Supports. To determine the membrane state under various operating conditions, we could use the theoretical model to calculate the energies of the membrane states under the specified conditions and determine which state is more energy favorable. As shown in eqs 4 and 5, the energy values were determined using the size of $E_{SLB-silica}$, E_{bend}, and geometry factors. Varying the size of $E_{SLB-silica}$, E_{bend}, and geometry factors can make the energetically favorable state of the system change. $E_{SLB-silica}$ can be significantly influenced by buffer ionic strength according to the extended DLVO theory, and E_{bend} can be substantially influenced by the lipid membrane bending constant according to the Helfrich bending theory, and geometry factors are based on the used support geometry. Because the ionic strength, the lipid membrane composition, and the support geometry are the important physiologically or operationally relevant parameters varying from systems to systems, we demonstrated a theoretical membrane state map on an ionic strength versus bending constant diagram and showed how the map changes with support geometry, as shown in Figure 2.

To derive the theoretical membrane state regions in the ionic strength versus bending constant plot, we first drew the overall energies of CF and FS states under various ionic strength conditions for a given fixed bending constant (top, Figure 2). The three diagrams in the top panel were obtained with three different support geometries. In each plot, the three colored regions represent the different energetically favorable membrane states. In the pink region, poor formation of SLBs can be observed because the energy of both states was larger than zero and the SLB formation was not energetically favorable. As shown in the green region, the energy of the FS state was lower than that of the CF state; therefore, the FS state was more stable. The situation is the opposite in the blue region. The boundary of the blue and green regions occurred at a critical ionic strength at which the energies of the FS and CF states were the same. By varying bending constants and determining all of the critical ionic strengths, we mapped the FS and CF regions on ionic strength versus bending constant diagrams.

Figure 2 also shows that the CF region became larger when we increased the trench height (h) and kept the trench periodicity (w_1 and w_2) relatively similar. The reason is that when w_1 values were similar, the W_{FS} curves (green lines) of the three geometries were similar, as shown in eq 5 and the top panel plots in Figure 2. However, the W_{CF} curves (blue lines) shift downward in the plots when the trench height increases, which can be explained using eq 4. The combination resulted in the intersection of the two lines (the critical ionic strength), shifting to lower ionic strength; therefore, the CF region became larger.

In order to compare the consistency of the model prediction with the experiment result, we used the parameters in the range of our experimental conditions to obtain the theoretical membrane state maps in Figure 2. In the experiments, we varied ionic strength from 0 to 200 mM and used four different types of lipid, SOPC/Chol (2:3 mol/mol) (at 37 °C), DPPC (at 43 °C), DOPC (at 37 °C), and DMPC (at 37 °C). The lipid membranes composed the four different types of lipids at the specified temperatures have bending constants ranging from 0.7 to 3.4 ($\times 10^{-19}$) J. A fluorescently labeled lipid, Texas-Red DHPE, was incorporated into all of the lipid membranes, so that we can use fluorescence recovery after photobleaching technique to measure the diffusivities of the membranes. Since Texas-Red DHPE (TR-DHPE) is negatively charged, we incorporated different molar ratios of TR-DHPE into the four types of lipid membranes to make them have the same membrane surface charge density. To achieve the same membrane surface charge density, we considered the lipid headgroup areas of the various types of lipid membranes and incorporated 0.78 mol % TR-DHPE into 2:3 SOPC/Chol membranes (0.49 nm^2), 1.17 mol % TR-DHPE into DPPC membranes (0.64 nm^2), 1.35 mol % TR-DHPE into DOPC membranes (0.74 nm^2), and 1.09 mol % TR-DHPE in DMPC membranes (0.60 nm^2) to make the lipid membrane surface charge density (σ) equal to 0.0029 C/m^2. Figure 3 shows SEM images of the three fabricated supports we used in our experiments. The different heights (h) were obtained by treating the supports with different etching times (3, 4.5, and 6 min) during the fabrication processes. The curvature R was approximately 50 nm for all of the geometries. Note that although the same mode was used to imprint the features on the three supports, we obtained a slight variation of w_1 and w_2, which was caused by the instability of the heating history of the nanoimprinting instrument. With all of the parameters based on the experimentally operating conditions, we calculated W_{FS} and W_{CF} and generated the maps shown in Figure 2. The calculation details and all of the parameters we used can be found in the Supporting Information.

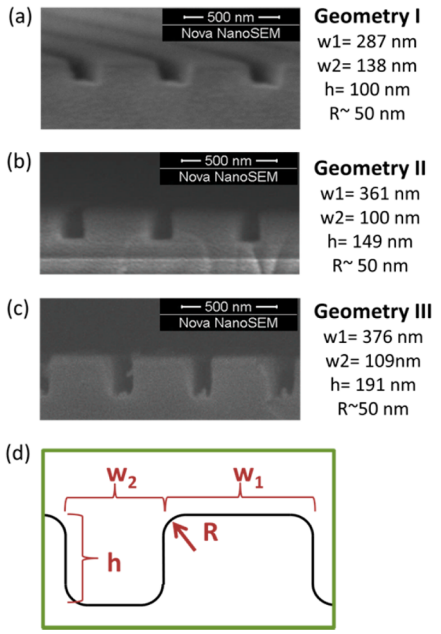

Figure 3. (a–c) SEM images and geometry information on the three types of nanograting structure fused silica. (d) Illustration of the geometry symbols.

Examining Experimental Membrane States Using 2D Fluorescence Recovery after Photobleaching (FRAP) Measurement. Our goal was to experimentally verify that

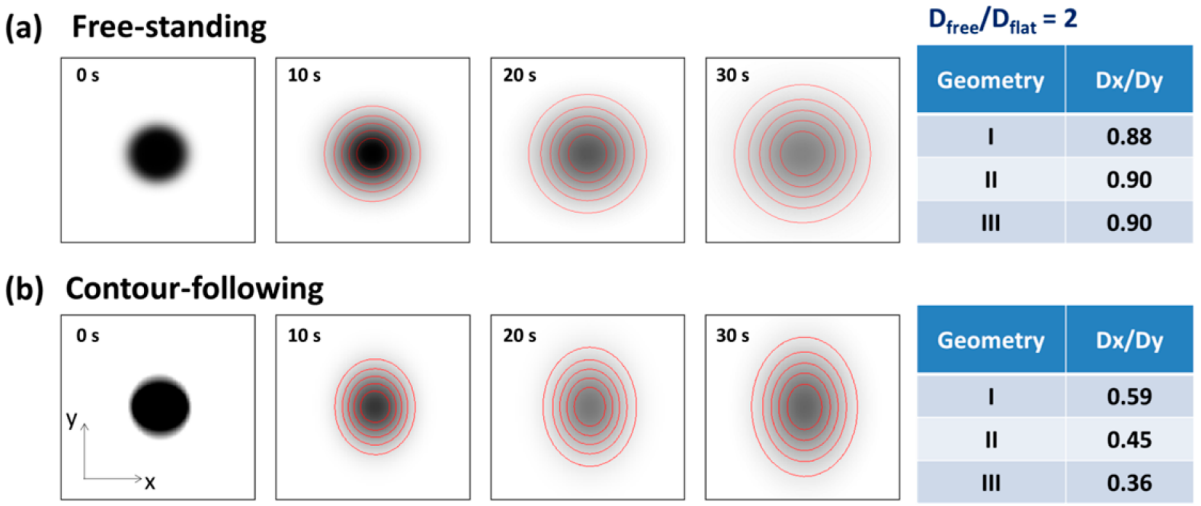

Figure 4. COMSOL simulation of the fluorescence recovery after photobleaching for (a) FS and (b) CF states on the nanograting supports. The left evolution images show the simulated recovery for the Geometry I support. The x axis is perpendicular to the grating structure, and the y axis is parallel to the structure. The dark color indicates the bleached region, and the red lines are the intensity contour regression lines obtained by fitting the intensity profile to the 2D transport equation. Right panels show the D_x/D_y values of the three supports calculated from the simulation recovery results.

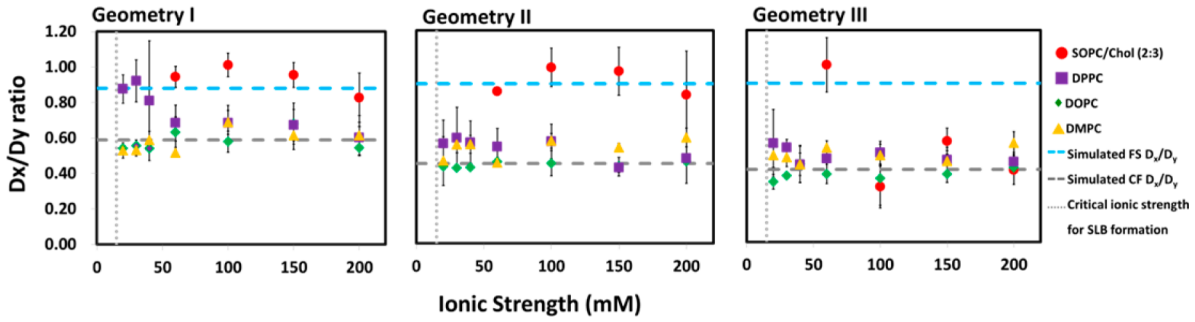

Figure 5. D_x/D_y values of SOPC/Chol (2:3 mol/mol), DOPC, DPPC, and DMPC under various ionic strengths and on the three different nanograting size fused silica supports with Geometries I, II, and III.

the developed model can estimate membrane states. After obtaining the CF and FS membrane state regions in the ionic strength versus bending constant diagram estimated by the model, we experimentally prepared membranes under various conditions and observed their states. However, because of the nano size, it was difficult to distinguish the membrane states; therefore, we developed a method to experimentally determine the membrane state by qualitatively observing the fluorescence recovery shape change. For a conventional SLB on a planar support, the isotropic fluorescence recovery can be observed after a laser bleaches a circular spot on the membrane. However, when an SLB is on the trenched support, anisotropic fluorescence recovery can be observed because the lengths of the diffusion paths in the direction along the trenches and in the direction perpendicular to the trenches are different.

We used COMSOL numerical simulation software to predict various recovery scenarios when the lipid membrane was in FS or CF states, assuming that the lipid diffusion in the lipid bilayer can be accurately described using the 2D classical transport equation. Figure 4 demonstrates how the recovery shape would change with time. The different shape changes of the two states can be used to distinguish the experimental membrane states. For the FS membrane state we defined the diffusion coefficient of the lipid membrane on a solid support as D_{flat} and that of the free lipid membrane without support interaction as D_{free}. Previous studies have reported that D_{free}/D_{flat} is approximately 2.5.[15,22] In our study, we determined the D_{free}/D_{flat} value approximately to be 2. Using this number, the simulation result of the D_x/D_y values for the FS state membrane on the three different supports is shown in the right panel of Figure 4a. For the CF state, D_x/D_y values were substantially influenced by the trench height, and the simulation result is shown in the right panel of Figure 4b. The simulation details of how we obtained the D_x/D_y values for both membrane states are presented in the Supporting Information.

Experimental Membrane States Influenced by Bending Constant, Ionic Strength, and the Nanograting Structure. To determine whether the experimental membrane states matched the membrane state regions predicted using the developed model, we prepared four different types of lipid, DOPC, DMPC, DPPC, and SOPC/Chol (2:3 mol/mol), to construct membranes with various bending constants, ranging from 0.7 to 3.4 ($\times 10^{-19}$) J,[37] and conducted experiments on supports with various geometries under various ionic strengths. To determine the experimental membrane states, we collected their FRAP data and obtained their D_x and D_y by fitting the FRAP data to the 2D classical mass transport equation (details in the Methods section and Supporting Information). Figure 5 shows the fitted D_x/D_y ratios of all of our experiments conducted with the four types of lipid membrane under ionic

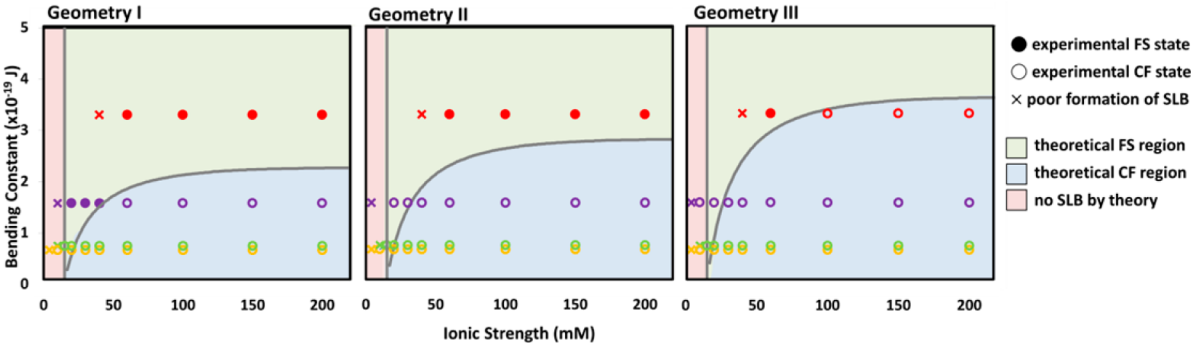

Figure 6. Comparison of the experimental membrane states and the model prediction on a bending constant versus ionic strength diagram. Filled dots represent the experimental FS state, and hollow dots represent the experimental CF state. Red, purple, green, and yellow dots represent the experimental data from SLBs composed of SOPC/Chol (2:3 mol/mol), DPPC, DOPC, and DMPC, respectively. Light green, light blue, and pink regions represent the theoretically predicted FS state region, CF state region, and no SLB formation region.

strength conditions varying from 20 to 200 mM on the three types of nanograting support shown in Figure 3a, 3b, and 3c. All of our experiments were operated, and the diffusivities were measured at temperatures higher than the transition temperatures of the used lipids to ensure than the lipid membranes were in their fluid states. We used a physiologically relevant temperature of 37 °C for the DOPC, DMPC, and SOPC/Chol (2:3 mol/mol) membranes and 43 °C for the DPPC membrane to ensure the temperature is above its transition temperature.

To determine whether the experimental membrane state was FS or CF, we compared the fitted D_x/D_y ratios with the simulated D_x/D_y values from COMSOL numerical software. The simulated values of the CF state and FS state are shown as gray dashed lines and black dotted lines, respectively, in Figure 5. As shown in Figure 5, the most rigid lipid membrane composed of SOPC/Chol (2:3 mol/mol) had a D_x/D_y value close to the simulated FS D_x/D_y value for the entire tested ionic strength range on both the Geometry I and the Geometry II supports. However, on the Geometry III support, which has the largest trench height (h), the SOPC/Chol (2:3 mol/mol) lipid membrane had a D_x/D_y value close to the simulated FS D_x/D_y value only under low ionic strength conditions, and the D_x/D_y values became similar to the simulated CF D_x/D_y value under high ionic strength conditions. The second most rigid lipid membrane composed of DPPC had D_x/D_y values similar to the simulated FS D_x/D_y values under low ionic strength conditions, 20−40 mM, and the values started to approach the simulated CF D_x/D_y value above 60 mM. In the supports with higher trench height (Geometries II and III), we observed that all of the D_x/D_y values under the entire ionic strength range were close to the simulated CF D_x/D_y values. For the softer lipid membrane composed of either DMPC or DOPC, D_x/D_y remained close to the simulated CF D_x/D_y values for the entire ionic strength range and on all of the supports we tested.

Comparison of the Experimental Membrane States and the Model Predictions. After determining the possible experimental membrane states, as shown in Figure 5, we mapped them to the corresponding locations in the predicted membrane state diagrams, as shown in Figure 6. The filled dots indicate the experimental FS membrane state, and the unfilled dots represent the experimental CF membrane state. Note that the location of the theoretical dividing line between the FS region and the CF region slightly varies with lipid type. We found that the dividing line shifts toward the higher bending constant region when we used the parameters of a more rigid lipid and toward the lower bending constant region when we used the parameters of a softer lipid. The locations of the representative theoretical dividing lines shown in Figure 6 were obtained by averaging those of a representative rigid type of lipid, DPPC, and of a representative soft type of lipid, DOPC.

Figure 6 demonstrates consistency between the experimental results and the predicted membrane state regions for all of the support types. The consistency suggested that the model can be used to predict membrane states accurately, based on experimentally controllable conditions, such as ionic strength, bending constant, and solid support geometry. Qualitatively, if the lipid type and buffer ionic strength are fixed, the free-standing state can occur when the support geometry has more bending edges compared with the surface area where the membrane contacts. If the support geometry is fixed, the FS state can occur when using a lipid membrane with a higher bending constant at a lower ionic strength. Quantitatively, the model can estimate whether a certain set of experimental conditions can be used to create FS lipid membranes.

Our study suggests a guideline to choose suitable lipid types, buffer ionic strengths, and support geometries to make the spanning membrane state (FS state) become the energetically favorable state. Previous studies have suggested that using lipid vesicles with diameters larger than the pore is a necessary but not sufficient condition for the pore-spanning membrane formation.[20,21] They also show that the percentage of successfully spanned pores depends on the frequency of occurrence of a vesicle positioning itself over the pore region during the vesicle deposition method; therefore, the maximum spanned fraction is close to the critical surface coverage, which causes vesicle rupture. We used the lipid vesicles extruded from 50 nm polycarbonate membranes to form SLBs on supports with trench widths larger than 100 nm and found the successful formation of trench-spanning SLBs. Our result shows that it is possible to use vesicles similar or smaller than the support structure size to form spanning SLBs, as long as the operating conditions are properly chosen to make the FS membrane state become the energetically favorable state. In addition, the result also suggests that the maximum achieved spanned fraction by the vesicle deposition method would not be limited by the critical surface coverage for vesicle rupture if proper operating conditions are used. On the other hand, Hook et al. found that an FS membrane on a silica substrate can be observed at a high pH value (pH = 9.5) and that the membrane followed the support contour at pH = 8. Their observation can be explained using our theoretical model. It has been shown that the negative surface charge of a silica surface at pH = 9.5 can be

twice that at pH = 8.[38] If the surface charge increases, the SLB−silica electrostatic repulsion can become larger, causing $E_{SLB-silica}$ to become smaller; therefore, the critical ionic strength for W_{FS} to be smaller than W_{CF} is shifted to larger value, and the FS stable region become larger. When all of the other conditions (E_{bend}, the geometry factor, and other properties) are kept constant, it is possible that the CF state is the more energetically favorable one at pH = 8, whereas the FS state becomes more energetically favorable at pH = 9.5.

Note that we incorporated negatively charged Texas-Red DHPE into the lipid membranes; therefore, both the lipid membranes and the silica surface are negatively charged under the experimental conditions we used. In the extended DLVO theory, the charge−charge surface interaction can be well described by the electrostatic interaction energy (E_{EDL}) with the expression shown in eq 7. However, if a neutral lipid membrane and a charged support surface are used, we think the electrostatic interaction term (E_{EDL}) in the model could be replaced by the interaction between the charged surface and the zwitterionic dipole surface ($E_{charge-dipole}$). Although the analytical expression of $E_{charge-dipole}$ in SLBs is still unclear, the charge−dipole interaction ($E_{charge-dipole}$) should be always smaller than the charge−charge interaction (E_{EDL}). From a typical energy plot as shown in Figure 1(a), Supporting Information, replacing E_{EDL} to smaller $E_{charge-dipole}$, while the van der Waals interaction energy (E_{vdw}) and hydration interaction energy (E_H) remain the same, could result in the increase of $E_{SLB-silica}$ and decrease of the water layer thickness.

CONCLUSION

In this study, we developed a theoretical model to estimate the appropriate conditions for creating FS lipid bilayers on solid supports with a nanograting structure. The model determines whether the FS or the CF membrane state is more energetically favorable under various conditions by evaluating the system energies of the states. We used the extended DLVO theory and the Helfrich bending theory to correlate the system energies and experimentally controllable parameters. To experimentally examine whether the membrane state follows the model prediction, we prepared samples composed of lipids with various bending constants ranging from 0.7 to 3.3 ($\times 10^{-19}$) J and conducted experiments under a range of ionic strength conditions (from 5 to 200 mM NaCl) on supports with three different nanograting geometries. Characterization of experimental membrane states using fluorescence recovery after photobleaching measurement revealed that all of our experiment results closely matched the theoretical predictions and that the developed theory could be used to predict the suitable conditions for FS bilayers.

ASSOCIATED CONTENT

Supporting Information

Supporting figures and data analyses. This material is available free of charge via the Internet at http://pubs.acs.org.

AUTHOR INFORMATION

Corresponding Author

*E-mail: lingchao@ntu.edu.tw.

Notes

The authors declare no competing financial interest.

ACKNOWLEDGMENTS

We thank Prof. Cheng-Che Hsu for use of the Comsol software in his lab. We thank National Taiwan University and the National Science Council in Taiwan for funding support for this work (NSC100-2218-E-002-023-MY2 and NSC102-2221-E-002-153-MY3).

ABBREVIATIONS

SOPC, 1-stearoyl-2-oleoyl-*sn*-glycero-3-phosphocholine; Chol, cholesterol; DOPC, 1,2-dioleoyl-*sn*-glycero-3-phosphocholine; DMPC, 1,2dimyristoyl-sn-glycero-3-phosphocholine; DPPC, 1,2-dipalmitoyl-sn-glycero-3-phosphocholine

REFERENCES

(1) Steinem, C.; Janshoff, A.; Ulrich, W.-P.; Sieber, M.; Galla, H.-J. Impedance Analysis of Supported Lipid Bilayer Membranes: A Scrutiny of Different Preparation Techniques. *Biochim. Biophys. Acta* **1996**, *1279*, 169−180.

(2) Nielsen, L. K.; Vishnyakov, A.; Jorgensen, K.; Bjornholm, T.; Mouritsen, O. G. Nanometre-Scale Structure of Fluid Lipid Membranes. *J. Phys.: Condens. Matter* **2000**, *12*, A309−A314.

(3) Salamon, Z.; Huang, D.; Cramer, W. A.; Tollin, G. Coupled Plasmon-Waveguide Resonance Spectroscopy Studies of the Cytochrome B6f/Plastocyanin System in Supported Lipid Bilayer Membranes. *Biophys. J.* **1998**, *75*, 1874−1885.

(4) Reviakine, I.; Brisson, A. Formation of Supported Phospholipid Bilayers from Unilamellar Vesicles Investigated by Atomic Force Microscopy. *Langmuir* **2000**, *16*, 1806−1815.

(5) Keller, C. A.; Kasemo, B. Surface Specific Kinetics of Lipid Vesicle Adsorption Measured with a Quartz Crystal Microbalance. *Biophys. J.* **1998**, *75*, 1397−1402.

(6) Kiessling, V.; Tamm, L. K. Measuring Distances in Supported Bilayers by Fluorescence Interference-Contrast Microscopy: Polymer Supports and Snare Proteins. *Biophys. J.* **2003**, *84*, 408−418.

(7) Tamm, L. K. Lateral Diffusion and Fluorescence Microscope Studies on a Monoclonal Antibody Specifically Bound to Supported Phospholipid Bilayers. *Biochemistry* **1988**, *27*, 1450−1457.

(8) Dietrich, C.; Merkel, R.; Tampe, R. Diffusion Measurement of Fluorescence-Labeled Amphiphilic Molecules with a Standard Fluorescence Microscope. *Biophys. J.* **1997**, *72*, 1701−1710.

(9) Salafsky, J.; Groves, J. T.; Boxer, S. G. Architecture and Function of Membrane Proteins in Planar-Supported Bilayers: A Study with Photosynthetic Reaction Centers. *Biochemistry* **1996**, *35*, 14773−14781.

(10) Hook, F.; Kasemo, B.; Nylander, T.; Fant, C.; Sott, K.; Elwing, H. Variations in Coupled Water, Viscoelastic Properties, and Film Thickness of a Mefp-1 Protein Film During Adsorption and Cross-Linking: A Quartz Crystal Microbalance with Dissipation Monitoring, Ellipsometry, and Surface Plasmon Resonance Study. *Anal. Chem.* **2001**, *73*, 5796−5804.

(11) Demarche, S.; Sugihara, K.; Zambelli, T.; Tiefenauer, L.; Vörös, J. Techniques for Recording Reconstituted Ion Channels. *Analyst* **2011**, *136*, 1077−1089.

(12) Mueller, P.; Rudin, D. O.; Ti Tien, H.; Wescott, W. C. Reconstitution of Cell Membrane Structure in Vitro and Its Transformation into an Excitable System. *Nature* **1962**, *194*, 979−980.

(13) Mueller, P.; Rudin, D. O.; Tien, H. T.; Wescott, W. C. Methods for the Formation of Single Bimolecular Lipid Membranes in Aqueous Solution. *J. Phys. Chem.* **1963**, *67*, 534−535.

(14) Castellana, E. T.; Cremer, P. S. Solid Supported Lipid Bilayers: From Biophysical Studies to Sensor Design. *Surf. Sci. Rep.* **2006**, *61*, 429−444.

(15) Kocun, M.; Lazzara, T. D.; Steinem, C.; Janshoff, A. Preparation of Solvent-Free, Pore-Spanning Lipid Bilayers: Modeling the Low Tension of Plasma Membranes. *Langmuir* **2011**, *27*, 7672−7680.

(16) Heinemann, F.; Schwille, P. Preparation of Micrometer-Sized Free-Standing Membranes. *ChemPhysChem* **2011**, *12*, 2568−2571.

(17) Kleefen, A.; Pedone, D.; Grunwald, C.; Wei, R.; Firnkes, M.; Abstreiter, G.; Rant, U.; Tampé, R. Multiplexed Parallel Single Transport Recordings on Nanopore Arrays. *Nano Lett.* **2010**, *10*, 5080−5087.
(18) Kresak, S.; Hianik, T.; Naumann, R. L. C. Giga-Seal Solvent-Free Bilayer Lipid Membranes: From Single Nanopores to Nanopore Arrays. *Soft Matter* **2009**, *5*, 4021−4032.
(19) Lazzara, T. D.; Carnarius, C.; Kocun, M.; Janshoff, A.; Steinem, C. Separating Attoliter-Sized Compartments Using Fluid Pore-Spanning Lipid Bilayers. *ACS Nano* **2011**, *5*, 6935−6944.
(20) Claesson, M.; Frost, R.; Svedhem, S.; Andersson, M. Pore Spanning Lipid Bilayers on Mesoporous Silica Having Varying Pore Size. *Langmuir* **2011**, *27*, 8974−8982.
(21) Kumar, K.; Isa, L.; Egner, A.; Schmidt, R.; Textor, M.; Reimhult, E. Formation of Nanopore-Spanning Lipid Bilayers through Liposome Fusion. *Langmuir* **2011**, *27*, 10920−10928.
(22) Jönsson, P.; Jonsson, M. P.; Höök, F. Sealing of Submicrometer Wells by a Shear-Driven Lipid Bilayer. *Nano Lett.* **2010**, *10*, 1900−1906.
(23) Werner, J. H.; Montaño, G. A.; Garcia, A. L.; Zurek, N. A.; Akhadov, E. A.; Lopez, G. P.; Shreve, A. P. Formation and Dynamics of Supported Phospholipid Membranes on a Periodic Nanotextured Substrate. *Langmuir* **2009**, *25*, 2986−2993.
(24) Jonsson, M. P.; Jönsson, P.; Dahlin, A. B.; Höök, F. Supported Lipid Bilayer Formation and Lipid-Membrane-Mediated Biorecognition Reactions Studied with a New Nanoplasmonic Sensor Template. *Nano Lett.* **2007**, *7*, 3462−3468.
(25) Furukawa, K.; Sumitomo, K.; Nakashima, H.; Kashimura, Y.; Torimitsu, K. Supported Lipid Bilayer Self-Spreading on a Nanostructured Silicon Surface. *Langmuir* **2006**, *23*, 367−371.
(26) Suzuki, K.; Masuhara, H. Groove-Spanning Behavior of Lipid Membranes on Microfabricated Silicon Substrates. *Langmuir* **2005**, *21*, 6487−6494.
(27) Cremer, P. S.; Boxer, S. G. Formation and Spreading of Lipid Bilayers on Planar Glass Supports. *J. Phys. Chem. B* **1999**, *103*, 2554−2559.
(28) Oleson, T. A.; Sahai, N. Interaction Energies between Oxide Surfaces and Multiple Phosphatidylcholine Bilayers from Extended-Dlvo Theory. *J. Colloid Interface Sci.* **2010**, *352*, 316−326.
(29) Nabika, H.; Fukasawa, A.; Murakoshi, K. Control of the Structure of Self-Spreading Lipid Membrane by Changing Electrolyte Concentration. *Langmuir* **2006**, *22*, 10927−10931.
(30) Tero, R.; Ujihara, T.; Urisu, T. Lipid Bilayer Membrane with Atomic Step Structure: Supported Bilayer on a Step-and-Terrace Tio2 (100) Surface. *Langmuir* **2008**, *24*, 11567−11576.
(31) Helfrich, W. Elastic Properties of Lipid Bilayers: Theory and Possible Experiments. *Z. Naturforsch., C: Biochem., Biophys., Biol., Virol.* **1973**, *28*, 693.
(32) Zimmerberg, J.; Kozlov, M. M. How Proteins Produce Cellular Membrane Curvature. *Nat. Rev. Mol. Cell Biol.* **2005**, *7*, 9−19.
(33) Petrache, H. I.; Zemb, T.; Belloni, L.; Parsegian, V. A. Salt Screening and Specific Ion Adsorption Determine Neutral-Lipid Membrane Interactions. *Proc. Natl. Acad. Sci. U.S.A.* **2006**, *103*, 7982−7987.
(34) Israelachvili, J. N. *Intermolecular and Surface Forces*, 3rd ed.; Academic press: San Diego, CA, 2011.
(35) McIntosh, T.; Simon, S. Hydration Force and Bilayer Deformation: A Reevaluation. *Biochemistry* **1986**, *25*, 4058−4066.
(36) Israelachvili, J.; Pashley, R. The Hydrophobic Interaction Is Long Range, Decaying Exponentially with Distance. *Nature* **1982**, *300*, 341−342.
(37) Marsh, D. Elastic Curvature Constants of Lipid Monolayers and Bilayers. *Chem. Phys. Lipids* **2006**, *144*, 146−159.
(38) Fukuzaki, S.; Urano, H.; Nagata, K. Adsorption of Bovine Serum Albumin onto Metal Oxide Surfaces. *J. Ferment. Bioeng.* **1996**, *81*, 163−167.